Scale Dependent Analytical Investigation of the Dynamic State Index Concerning the Quasi-Geostrophic Theory

Annette Müller* and Peter Névir†

Institut für Meteorologie, Freie Universiät Berlin

Rupert Klein

Institut für Mathematik, Freie Universität Berlin

**Corresponding author address:* Annette Müller, Institut für Meteorologie, Carl-Heinrich-Becker-Weg 6-10, 12165 Berlin, Germany.

E-mail: annette.mueller@met.fu-berlin.de

†Institut für Meteorologie, Carl-Heinrich-Becker-Weg 6-10, 12165 Berlin, Germany

ABSTRACT

The Dynamic State Index (DSI) is a scalar diagnostic field that quantifies local deviations from a steady and adiabatic wind solution and thus indicates non-stationarity as well as diabaticity. The DSI-concept has originally been developed through the Energy-Vorticity Theory based on the full compressible flow equations without regard to the characteristic scale-dependence of many atmospheric processes. Such scale-dependent information is often of importance, and particularly so in the context of precipitation modeling: Small scale convective events are often organized in storms, clusters and "Großwetterlagen" across a wide range of scales. A concrete example shows that, by combining the DSI concept with ideas of scale analysis, one can derive new scale-dependent DSI-like indicators that distinguish the different levels of organization in precipitation systems.

The example consists of (i) developing a DSI index for the quasi-geostrophic model using the Energy-Vorticity Theory, (ii) showing that it is asymptotically consistent with the original index for the primitive equations, and (iii) evaluating both indices for meteorological reanalysis data to demonstrate that they capture systematically different scale-dependent precipitation information.

A spin-off of the asymptotic analysis is a novel non-equilibrium time scale combining potential vorticity and the DSI indices. Its possible ramifications for turbulence modeling across a wide range of atmospheric scales is briefly mentioned.

1. Introduction

Meteorological observations and numerical flow simulations are often interpreted in terms of "anomalies" of dynamic variables. Typically, these are obtained as local deviations from large-scale space, time, or ensemble mean states, (see, e.g., Martius et al. 2016; Allan and Soden 2008; Saji et al. 1999), and their structure is taken to be indicative of ongoing dynamic processes. A somewhat unsatisfactory aspect of this approach is that the meteorological interpretation of the underlying mean states is generally rather difficult: Neither can the time series of such mean states be expected to constitute flow solutions all by themselves, nor does any instantaneous mean state have particular meteorologically distinct features that would justify its use as a reference for measuring anomalies. Hence, although such analyses of anomalies have undoubtedly proven useful in pragmatic terms, a theoretically interesting question remains: What is the proper physical interpretation of the distance between an observed or simulated state on the one hand, and such an averaged but otherwise not really distinct state on the other?

The Dynamic State Index (DSI), the definition of which is given in (11) below, is a quantitative scalar indicator for ongoing nonstationary, diabatic, and dissipative processes that avoids this uncertainty of interpretation. It is a parameter based on first principles of fluid mechanics (Névir 2004; Névir and Sommer 2009) that locally quantifies non-stationarity, diabaticity, and viscous dissipation in a solution of the primitive equations without relying on a reference field. While the index thus has a mathematically precise definition and physically clear interpretation, it has at least two shortcomings in comparison with the, generally multivariate, anomalies: First, it melds three process properties into a single scalar, leaving unaddressed the question which of the properties is how important in any given situation. Secondly, being a local quantity obtained from point-wise evaluated gradients of the primary flow variables, it does not reveal any information on the scale-dependence of the indicated processes. In the present paper we begin to address the second issue by demonstrating how scale-dependent versions of the index reveal features of organization of precipitation on different spacio-temporal scales.

So far, the DSI based on the primitive equations ($\mathrm{DSI_{PE}}$) has been applied to data sets with different resolutions for different scales (Gaßmann 2014; Claussnitzer and Névir 2009; Claussnitzer et al. 2011). On synoptic scales, using ECMWF's ERA-40 Reanalysis data set, it has been shown that the DSI indicates waves and vortices caused by baroclinic instability. On the meso-scale, the DSI field can be applied to detect hurricanes as discussed in Weber and Névir (2008). On this scale cyclones, hurricanes and storms become visible as DSI dipole structures. As an example, these authors illustrated the dipole structures of the storm Lothar in December 26, 1999 and of hurricane Andrew in August 1992. Finally, on convective scales the DSI indicates cumulonimbus clouds with strong updrafts within the associated elongated frontal precipitation bands. Thus, Claussnitzer et al. (2008) and Weijenborg et al. (2015) found that the DSI is strongly correlated with intense convective precipitation processes.

Thus, there is clear evidence that the $\mathrm{DSI_{PE}}$ highlights different processes on different scales in data that are scale-filtered by limited numerical resolution. Yet, the interesting question of whether DSI-like quantities could be used to identify different processes that are simultaneously active on different scales in high resolution simulations or observations remains open. The present paper documents our first steps towards resolving this issue.

In section 2 we recall the derivation of the DSI for the primitive equations based on arguments of the Energy-Vorticity Theory. In section 3 we apply the same concepts to define a Dynamic State Index, $\mathrm{DSI_{QG}}$, for the quasi-geostrophic (QG) model which, by the nature of the QG theory, is indicative of non-stationarity, diabaticity, and dissipation in geostrophically balanced synoptic scale flows.

In section 4 we consider, in contrast, the asymptotics of the $\mathrm{DSI}_{\mathrm{PE}}$ in the quasi-geostrophic flow regime. The reassuring result is that its leading-order approximation is equivalent to the $\mathrm{DSI}_{\mathrm{QG}}$ derived in section 3, so that the $\mathrm{DSI}_{\mathrm{PE}}$ inherits the clear physical interpretation of the $\mathrm{DSI}_{\mathrm{QG}}$ when applied to geostrophically balanced flows. An interesting additional aspect of the asymptotics is the extreme rescaling of the $\mathrm{DSI}_{\mathrm{PE}}$ amplitude with increasing spacio-temporal scales: If the $\mathrm{DSI}_{\mathrm{PE}}$ evaluated on the meso-gamma scale of ~ 10 km is taken as a reference, and $\varepsilon \ll 1$ is the synoptic flow Rossby number, then the $\mathrm{DSI}_{\mathrm{PE}}$ evaluated on synoptic-scale geostrophically balanced data scales as ε^{10}! While this can be traced back to straighforward scaling properties as explained in section 4, this extreme scaling implies that quite sophisticated data analysis techniques will have to be invoked (in future work) to robustly extract scale-dependent DSI-information from high-resolution multiscale flow fields. In section 5, in turn, we consider COSMO-DE Reanalyses data of precipitating flow fields, compare the output of the $\mathrm{DSI}_{\mathrm{PE}}$ with that of its quasi-geostrophic analogue, the $\mathrm{DSI}_{\mathrm{QG}}$, and interpret the results based on the foregoing analytical insights. Section 6 provides conclusions and an outlook to future work.

2. The Dynamic State Index for the primitive equation

Hitherto, the Dynamic State Index ($\mathrm{DSI}_{\mathrm{PE}}$) has been derived and analyzed only for the most comprehensive case, the system of primitive equations. This parameter quantifies how far local flow conditions deviate from stationarity, adiabaticity, and inviscid behavior (Névir 2004). A physically intuitive interpretation of the index in terms of Schär's steady wind expression (Schär 1993) is given here as follows: First, we will follow Weber and Névir (2008) and derive the steady wind in terms of the Energy-Vorticity Theory (EVT). The EVT for adiabatic, inviscid fluids treats the globally conserved quantities, energy and Ertel's PV, equally. Second, we will motivate the DSI in terms of this steady wind and the conservation of mass. And third, we will relate the

DSI, respectively the steady wind, to other meteorological fields commonly used in atmospheric dynamics and show that this index provides a tool to measure energy-vorticity imbalances.

a. Derivation of the $\mathrm{DSI_{PE}}$ *from the Energy-Vorticity Theory*

The total energy of an ideal fluid $\mathscr{H}$ is given by the sum of the kinetic, potential and internal part:

$$\mathscr{H} = \int_V d\tau\rho \left[\frac{1}{2}\mathbf{v}^2 + \phi + e(v,s)\right] \tag{1}$$

with density ρ, 3D velocity $\mathbf{v}$, potential of the external gravity field ϕ and specific internal energy $e(v,s)$ that depend on the specific volume v and the specific entropy s. Ertel's potential enstrophy $\mathscr{E}$ reads:

$$\mathscr{E} = \frac{1}{2}\int_V d\tau\Pi^2 \quad \text{with} \quad \Pi = \frac{\boldsymbol{\xi}_a \cdot \nabla s}{\rho} \tag{2}$$

where $\boldsymbol{\xi}_a = \nabla \times \mathbf{v} + 2\boldsymbol{\omega}$ is the absolute 3D vorticity vector with angular velocity of the earth $\boldsymbol{\omega}$. To derive the steady wind, we recall from Claussnitzer (2010) that a stationary fluid dynamical state can be expressed by minimizing the energy functional under the constraint of a prescribed total potential enstrophy. Technically, this may be expressed as

$$(\rho,\mathbf{v},s) = \underset{(\rho,\mathbf{v},s)}{\arg\min}\left(\mathscr{H}(\rho,\mathbf{v},s) - \lambda\mathscr{E}(\rho,\mathbf{v},s)\right), \tag{3}$$

where λ is the Lagrange multiplier corresponding to the constraint. With the functional derivatives

$$\left.\frac{\delta\mathscr{H}}{\delta\mathbf{v}}\right|_{\rho,s} = \rho\mathbf{v}, \quad \left.\frac{\delta\mathscr{H}}{\delta\rho}\right|_{\mathbf{v},s} = B, \quad \left.\frac{\delta\mathscr{E}}{\delta\mathbf{v}}\right|_{\rho,s} = \nabla\Pi \times \nabla s, \quad \left.\frac{\delta\mathscr{E}}{\delta\rho}\right|_{\mathbf{v},s} = -\frac{1}{2}\Pi^2, \tag{4}$$

the variational problem from (3) with respect to ρ leads to

$$B = \frac{1}{2}\mathbf{v}^2 + \phi + e + \frac{p}{\rho} = -\lambda\frac{1}{2}\Pi^2 \tag{5}$$

and with respect to $\mathbf{v}$ we obtain:

$$\rho\mathbf{v} = \lambda\nabla\Pi \times \nabla s \tag{6}$$

(Névir 2004). The last equation was also used by Blender (2005). Inserting (5) in (6) for the Lagrangian multiplier, λ, and noticing that the entropy is a function of potential temperature, leads to the 3D steady wind condition

$$\mathbf{v}_{st} = \frac{1}{\rho\Pi}\nabla\Theta \times \nabla B. \tag{7}$$

The steady wind was introduced by Schär (1993). To derive the Dynamic State Index, we recall the laws of conservation of Ertel's potential vorticity Π and of the potential temperature Θ along Lagrangian trajectories,

$$\begin{aligned} \frac{d\Pi}{dt} &= \frac{\partial\Pi}{\partial t} + \mathbf{v}\cdot\nabla\Pi = 0\,, \\ \frac{d\Theta}{dt} &= \frac{\partial\Theta}{\partial t} + \mathbf{v}\cdot\nabla\Theta = 0\,. \end{aligned} \tag{8}$$

For steady flows, the local time derivatives $\partial/\partial t$ vanish identically, so that the advection of the potential vorticity and the potential temperature vanishes under adiabatic, steady, inviscid conditions, i.e. $\mathbf{v}_{st}\cdot\nabla\Pi = \mathbf{v}_{st}\cdot\nabla\Theta = 0$. This leads to

$$\mathbf{v}_{st} = \alpha\ \nabla\Theta \times \nabla\Pi \tag{9}$$

with some scalar factor of proportionality α. The two stationary velocity representations (7) and (9) allow for a geometric interpretation on isotropic surfaces: Both the Bernoulli function and Ertel's PV are stream functions of stationary flows in the sense that the stationary wind blows along the isolines of these two scalar fields within isentropic surfaces, $\Theta =$ const., see fig. 1.

Obviously, (7) implies that in a steady flow the Bernoulli function, B, is also constant along particle trajectories, i.e., $\mathbf{v}_{st}\cdot\nabla B = 0$ as well. Using the second expression for $\mathbf{v}_{st}$ from (9) in this latter equation, we obtain a non-trivial local condition

$$\mathbf{v}_{st}\cdot\nabla B = \alpha\ (\nabla\Theta \times \nabla\Pi)\cdot\nabla B = 0\,. \tag{10}$$

This expression with $\alpha = -1/\rho$ is the Dynamic State Index defined by Névir (2004), where α is chosen such that the conservation of mass in Lagrangian coordinates (a,b,c) is included, i.e. $\mathrm{d}m = \rho\ \mathrm{d}x\mathrm{d}y\mathrm{d}z = \mathrm{d}a\mathrm{d}b\mathrm{d}c$:

$$\mathrm{DSI_{PE}} := \frac{1}{\rho}(\boldsymbol{\nabla}\Theta \times \boldsymbol{\nabla}B)\cdot\nabla\Pi = \frac{1}{\rho}\frac{\partial(\Theta,B,\Pi)}{\partial(x,y,z)} = \frac{\partial(\Theta,B,\Pi)}{\partial(a,b,c)}\,. \tag{11}$$

According to (10) and (8) the $\mathrm{DSI_{PE}}$ is zero under stationary, adiabatic, and inviscid flow conditions, and it implies that the advection terms for the potential temperature, for the Bernoulli function, and for the potential vorticity all vanish. In contrast, non-zero values of the $\mathrm{DSI_{PE}}$ quantify deviations from these conditions, albeit without allowing the user to distinguish how much of the deviation is due to non-stationarity, diabaticity, or viscous dissipation without further information.

b. Derivation of the $\mathrm{DSI_{PE}}$ *from the steady wind field*

Considering adiabatic, inviscid fluids an interesting interpretation of the $\mathrm{DSI_{PE}}$ follows by the vanishing of the divergence of Schär's steady wind (7). Regarding the conservation of mass via the continuity equation we obtain for the steady state:

$$\left(\frac{\partial\rho}{\partial t}\right)_{st} = -\nabla\cdot(\rho\mathbf{v}_{st}) = 0. \tag{12}$$

Thus, inserting the expression of Schär's steady wind $\mathbf{v}_{st}$, given in (7), we obtain:

$$-\boldsymbol{\nabla}\cdot\left(\frac{1}{\Pi}\boldsymbol{\nabla}\Theta\times\boldsymbol{\nabla}B\right) = \frac{1}{\Pi^2}\boldsymbol{\nabla}\Pi\cdot(\boldsymbol{\nabla}\Theta\times\boldsymbol{\nabla}B) = \frac{\rho}{\Pi^2}\mathrm{DSI_{PE}} = 0\,. \tag{13}$$

This shows that the $\mathrm{DSI_{PE}}$ is zero for adiabatic, inviscid and steady flows. Moreover, we note that the conservation of mass, now in Eulerian representation, is implicitly integrated in the definition of the Dynamic State Index.

c. *Illustration of the* $\mathrm{DSI}_{\mathrm{PE}}$ *from the synoptic point of view*

For illustration, the spatial structure of the DSI on the 330 K isentropic surface of some typical reanalysis field is shown in fig. 1, lower panel. It shows that the DSI can diagnose the North Atlantic storm track by a band of DSI-dipoles (Weber and Névir 2008). The figure shows how the diabatic, non-steady processes associated with the storm tracks lead to non-alignment of the PV and the Bernoulli function isolines within the $\Theta = 330\,\mathrm{K}$ surface. In the present case, the flow passes through a PV anomaly leading to negative and positive DSI values on the upstream and downstream of the flow. In typical frontal zones, the wind crosses the PV isolines leading to DSI-signals indicating high correlations of the DSI with precipitation processes (Claussnitzer et al. 2008).

One can ask which additional benefit is provided by the DSI, in particular in comparison to the PV. On the one hand, the PV is a constitutive quantity describing only the rotational part of the velocity field, whereas the DSI also incorporates energetic information through the Bernoulli function. Furthermore, by the incorporation of the kinetic energy via the Bernoulli function, the divergent part of the energy is included, which is not integrated in the PV. On the other hand, PV analysis generally requires the extraction of PV anomalies as deviations from some climatological mean state that is not uniquely defined. In contrast, the DSI is a local quantity that *is* uniquely defined, independently of such a background field, to quantify deviations from the steady wind conditions of the primitive equations.

We notice in passing that the physical dimension of the Dynamic State Index is $[\mathrm{DSI}] = [\Pi^2/T]$ (Π: potential vorticity, T: time), so that the combination Π^2/DSI of both fields can be interpreted as a local intrinsic time scale of a flow field. We leave an exploration of this aspect and a discussion of its implications for flow data analysis to future work.

3. A Dynamic State Index for the QG-Theory

a. The DSI-concept for models other than the primitive equations

The concept of the DSI can be generalized such that a DSI can be designed for arbitrary fluid mechanical models that describe the evolution of vortices. Regarding the different scales of atmospheric motion, it is of interest to consider especially the well-known reduced models. In general, different models lead to different stationary velocities and to different stream functions and vorticity related conserved quantities, so that establishing relations between the respective model-specific DSI-type quantities calls for some analytical effort. As a common property, if the adapted stream function and vorticity related quantity share their isolines within surfaces of constant entropy, the DSI for the investigated model should vanish. Moreover, the degree of deviation from such alignment of the isolines represents a measure for deviations from a stationary state. Any model-specific DSI-type field should be designed to reproduce this property.

To derive the DSI for some reduced model in terms of the energy-vorticity concept, the following steps are required: (i.) Derivation of the stream function, B_{red}, related to the model's steady wind solution; (ii.) Determination of the adapted potential vorticity, Π_{red}; (iii.) Identification of some advected scalar η_{red} that defines the material surfaces on which the dynamics takes place. Then, the DSI is given by the advection of the potential vorticity evaluated with the steady wind field, and this is represented as the Jacobi-determinant of the surface η_{red}, the stream function B_{red}, and the potential vorticity Π_{red} with respect to the Lagrangian, or mass-weighted, coordinates, (a,b,c), which imply mass conservation, i.e.,

$$\mathrm{DSI}_{\mathrm{red}} = \frac{\partial(\eta_{red}, \mathrm{B}_{\mathrm{red}}, \Pi_{\mathrm{red}})}{\partial(a,b,c)} = \frac{1}{\rho}\frac{\partial(\eta_{red}, \mathrm{B}_{\mathrm{red}}, \Pi_{\mathrm{red}})}{\partial(x,y,z)}, \tag{14}$$

where $\frac{1}{\rho}$ is the Jacobi determinant that mediates between volume increments of the Lagrangian coordinates (a,b,c) and the fixed reference cartesian coordinates (x,y,z).

b. Application of the concept to the QG-model

The benchmark theory for understanding the evolution of baroclinic waves and vortices on the synoptic scale leads to the quasi geostrophic model (see, e.g., Pedlosky 1992), which filters all acoustic and gravity wave modes from the dynamics. In this section we adapt the DSI-concept to this model and label the resulting parameter by $\mathrm{DSI_{QG}}$.

In developing a DSI-type index for the QG-model, we first replace Ertel's potential vorticity Π by the quasi-geostrophic potential vorticity,

$$\Pi_{red} = \Pi_{\mathrm{QG}} = \frac{1}{f_0}\left[\nabla_{\|}^2\phi + \frac{f_0^2}{\rho_0}\frac{\partial}{\partial z}\left(\frac{\rho_0}{N_z^2}\frac{\partial\phi}{\partial z}\right)\right] + f\,. \tag{15}$$

To derive $\mathrm{DSI_{QG}}$ in the framework of the Energy-Vorticity Theory under the general condition that $N_z(z)$ and $\rho_0(z)$ are non-trivial functions of the height coordinate z, we reformulate the Π_{QG} and use an adapted scalar product and spatial gradient

$$\Pi_{\mathrm{QG}} = \frac{1}{f_0}\left[\nabla_{\|}^2\phi + \left(\frac{N_z^2}{\rho_0^2 f_0^2}\right)\left[\frac{\rho_0(z) f_0^2}{N_z^2(z)}\frac{\partial}{\partial z}\left(\frac{\rho_0(z) f_0^2}{N_z^2(z)}\frac{\partial\phi}{\partial z}\right)\right]\right] + f\,, \tag{16}$$

where f_0 denotes the Coriolis parameter, $\zeta_a = \zeta + f$ the absolute vorticity, ϕ the geopotential perturbation field, N_z the Brunt Väisälä-frequency as stratification parameter and $\nabla_{\|}$ the horizontal gradient (see Pedlosky 1992; Klein 2010, and Appendix A2b below). We set $\alpha(z) := \rho_0(z) f_0^2 N_z^{-2}(z)$ and $\gamma := N_z^2 \rho_0^{-2} f_0^{-2}$ to simplify the expression of the potential vorticity for the QG-model:

$$\Pi_{\mathrm{QG}} = \frac{1}{f_0}\left[\nabla_{\|}^2\phi + \gamma\left[\alpha(z)\frac{\partial}{\partial z}\left(\alpha(z)\frac{\partial}{\partial z}\right)\right]\right] + f\,. \tag{17}$$

In the next step, we define the scalar product of two vectors $\mathbf{a}, \mathbf{b} \in \mathbb{R}^3$ and the gradient $\tilde{\boldsymbol{\nabla}}$ as follows:

$$\mathbf{a} \cdot \mathbf{b} := a_x b_x + a_y b_y + \frac{f_0^2}{\rho_0^2 N_z^4} a_z b_z \tag{18}$$

$$\tilde{\boldsymbol{\nabla}} := \left(\frac{\partial}{\partial x}, \frac{\partial}{\partial y}, \alpha(z) \frac{\partial}{\partial z} \right) \tag{19}$$

Using (17), (18) and (19) the total energy reads as

$$\mathscr{H}_{QG} = \frac{1}{2} \int_V \rho_0 \, \frac{\tilde{\boldsymbol{\nabla}}\phi \cdot \tilde{\boldsymbol{\nabla}}\phi}{f_0^2} d\tau = \frac{1}{2} \int_V \rho_0 \, \left[\left(\frac{\nabla_{||}\phi}{f_0} \right)^2 + \left(\frac{1}{N_z} \frac{\partial \phi}{\partial z} \right)^2 \right] d\tau = \mathscr{H}_{QG,kin} + \mathscr{H}_{QG,pot}. \tag{20}$$

This expression was also derived by Pedlosky (1992) and Névir and Sommer (2009). Thus, for QG-flows, the total energy is given by the sum of the kinetic and potential energy.

In the framework of Energy-Vorticity-Theory, we consider the functional derivatives of two globally conserved quantities, the energy and a vorticity-related quantity.

$$\mathscr{H}_{QG} = \frac{1}{2 f_0^2} \int_m \left(\tilde{\boldsymbol{\nabla}} \phi \right)^2 dm \tag{21}$$

with the mass element $dm = \rho_0 dxdydz \equiv \rho_0 d\tau$. The second conserved quantity is given by the potential enstrophy (Névir 1998):

$$\mathscr{E}_{QG} = \frac{1}{2} \int_m \Pi_{\mathrm{QG}}^2 \, dm = \frac{1}{2 f_0^2} \int_m \left(\tilde{\boldsymbol{\nabla}}^2 \phi \right)^2 dm. \tag{22}$$

Following Névir (1998) further, the functional derivatives of the energy and the potential enstrophy with respect to Π_{QG} are given by

$$\frac{\delta \mathscr{H}_{QG}}{\delta \Pi_{\mathrm{QG}}} = B_{\mathrm{QG}} = -\frac{\phi}{f_0} \quad \text{and} \quad \frac{\delta \mathscr{E}_{QG}}{\delta \Pi_{\mathrm{QG}}} = \Pi_{\mathrm{QG}}. \tag{23}$$

Finally, we observe that advection in the QG model is defined by the leading order horizontal flow, so that z may take the role of the the advected variable η_{red} in (14). Then, according to (14), the Dynamic State Index for the QG-model can be defined with respect to the advected quantity $\eta_{red} = \eta_{\mathrm{QG}} = z$, the "poor man's stream function" $B_{red} = B_{\mathrm{QG}} = -\phi f_0^{-1}$ and $\Pi_{red} = \Pi_{\mathrm{QG}}$, and up to some scalar factor μ by

$$\mathrm{DSI}_{\mathrm{QG},\mu} = \mu \frac{\partial(\eta_{\mathrm{QG}}, B_{\mathrm{QG}}, \Pi_{\mathrm{QG}})}{\partial(a,b,c)} = -\frac{\mu}{\rho_0 f_0} \frac{\partial(\phi, \Pi_{\mathrm{QG}})}{\partial(x,y)}. \tag{24}$$

with $dadbdc = \rho_0 dxdydz$. Owing to (16), this representation of the DSI for QG-flows only depends on the geopotential height field ϕ and its derivatives, *i.e.*, $\mathrm{DSI}_{\mathrm{QG}} = \mathrm{DSI}_{\mathrm{QG}}[\phi]$, which is a characteristic property of the QG-model. We observe that it is proportional to the advection of the quasi-geostrophic PV with respect to the geostrophic wind, which takes the role of the steady wind $\mathbf{v}_{st}$ in the QG-model (see also the discussion in section 4d, however). For $\mathrm{DSI}_{\mathrm{QG}} = 0$ the potential vorticity depends on the stream function $\Pi_{\mathrm{QG}} = \Pi_{\mathrm{QG}}(\phi)$. This relationship has already been discussed in the 80's, for example in the context of blockings (Butchart et al. 1989).

4. Asymptotic analysis of the DSI in the QG regime

Here we demonstrate that the $\mathrm{DSI}_{\mathrm{QG}}$ as defined on the basis of the energy-vorticity concept in the previous section is the leading-order asymptotic approximation of the full $\mathrm{DSI}_{\mathrm{PE}}$ in the quasi-geostrophic flow regime. Following established derivations of the QG model equations, we adopt the β-plane approximation and work with Cartesian coordinates to match the definition of the $\mathrm{DSI}_{\mathrm{PE}}$ in (11).

a. Characterization of the quasi-geostrophic flow regime

Following Pedlosky (1992); Klein (2010), the quasi-geostrophic flow regime is defined by a coupled limit of the external and internal wave Froude and Rossby numbers such that

$$\begin{aligned}
\mathrm{Fr} &= \frac{u_{\mathrm{ref}}}{c_{\mathrm{ext}}} &\sim&\ \varepsilon^{\frac{3}{2}} && \text{(external wave Froude number)} \\
\widetilde{\mathrm{Fr}} &= \frac{u_{\mathrm{ref}}}{c_{\mathrm{int}}} &\sim&\ \varepsilon && \text{(internal wave Froude number)} \\
\mathrm{Ro} &= \frac{u_{\mathrm{ref}}}{f_0 L_{\mathrm{syn}}} &\sim&\ \varepsilon && \text{(Rossby number)}
\end{aligned} \tag{25}$$

where u_{ref} is a typical horizontal flow velocity magnitude,

$$c_{\mathrm{ext}} = \sqrt{g h_{\mathrm{sc}}}\,, \qquad c_{\mathrm{int}} = N_{\mathrm{ref}} h_{\mathrm{sc}} = \sqrt{\frac{\Delta\Theta}{T_{\mathrm{ref}}}}\, c_{\mathrm{ext}} \sim \sqrt{\varepsilon}\, c_{\mathrm{ext}}\,, \tag{26}$$

are characteristic values of the external and internal wave speeds with N_{ref} a tropospheric reference value of the Brunt-Väisälä frequency, and

$$h_{\mathrm{sc}} = \frac{p_{\mathrm{ref}}}{g\rho_{\mathrm{ref}}}\,, \qquad L_{\mathrm{syn}} = \frac{N_{\mathrm{ref}}}{f_0} h_{\mathrm{sc}} = \frac{h_{\mathrm{sc}}}{\varepsilon^2} \tag{27}$$

are the pressure scale height and the horizontal synoptic scale, respectively. The original derivation also adopts the "β-plane expansion" for the Coriolis parameter, i.e., $f = f_0(1 + \varepsilon\beta(y/L_{\mathrm{syn}}))$, and this implies $L_{\mathrm{syn}}/L_{\mathrm{p}} \sim \varepsilon$, where L_{p} denotes the planetary scale.

b. Asymptotic scaling of the $\mathrm{DSI}_{\mathrm{PE}}$ *and comparison with the* $\mathrm{DSI}_{\mathrm{QG}}$

Here we utilize existing results of asymptotic analysis to describe which physical processes contribute predominantly to the $\mathrm{DSI}_{\mathrm{PE}}$ in the quasi-geostrophic flow regime.

In the sequel, dimensional quantities will be tagged by a * superscript while dimensionless variables are denoted by plain letters. Following (Pedlosky 1992; Klein 2010), the Exner pressure,

π, potential temperature, Θ, horizontal velocity $\boldsymbol{u}$, and vertical velocity w obey

$$
\begin{aligned}
\pi = \left(\frac{p^*}{p_{\text{ref}}}\right)^{\frac{\kappa-1}{\kappa}} &= \pi_0 + \varepsilon\pi_1 + \varepsilon^2\pi^{(2)} + \mathscr{O}\left(\varepsilon^2\right) \\
\Theta = \frac{\Theta^*}{T_{\text{ref}}} &= \Theta_0 + \varepsilon\Theta_1 + \varepsilon^2\Theta^{(2)} + \mathscr{O}\left(\varepsilon^2\right) \\
\boldsymbol{u} = \frac{\boldsymbol{u}^*}{u_{\text{ref}}} &= \boldsymbol{u}^{(0)} + \mathscr{O}(1) \\
w = \frac{w^*}{u_{\text{ref}}} &= \varepsilon^3 w^{(3)} + \mathscr{O}\left(\varepsilon^3\right)
\end{aligned}
\tag{28}
$$

with the isentropic exponent

$$
\kappa = \frac{c_p}{c_v} \tag{29}
$$

where c_p and c_v are the heat capacities at constant pressure and volume, respectively. Considering (28), except for $\Theta_0 \equiv 1$, the background state variables (π_0, π_1, Θ_1), which we label by subscripts in counting their expansion orders, depend on the vertical coordinate z only. The super-scripted quantities $\left(\pi^{(2)}, \Theta^{(2)}, \boldsymbol{u}^{(0)}, w^{(3)}\right)$ are functions of the dimensionless independent variables

$$
\tau = \frac{t^* u_{\text{ref}}}{L_{\text{syn}}}, \qquad (\xi_1, \xi_2) = \boldsymbol{\xi} = \frac{\boldsymbol{x}^*}{L_{\text{syn}}} = \frac{(x^*, y^*)}{L_{\text{syn}}}, \qquad z = \frac{z^*}{h_{\text{sc}}}. \tag{30}
$$

We will use this notation in the sequel to distinguish between purely z-dependent variables $\Psi_i(z)$ and variables that depend on the full set of coordinates $\Psi^{(i)}(\tau, \boldsymbol{\xi}, z)$. Below, $\nabla_{\boldsymbol{\xi}} = (\partial_{\xi_1}, \partial_{\xi_2})$ denotes the horizontal gradient with respect to the $\boldsymbol{\xi}$-coordinates. Since the vertical (z) and horizontal (ξ_1, ξ_2) coordinates are scaled by different reference lengths h_{sc} and $L_{\text{syn}} = h_{\text{sc}}/\varepsilon^2$, respectively, the dimensional gradient operator used in expressing the DSI_{PE} in section 2 reads

$$
\nabla = \frac{1}{h_{\text{sc}}}\left(\varepsilon^2\frac{\partial}{\partial\xi_1}, \varepsilon^2\frac{\partial}{\partial\xi_2}, \frac{\partial}{\partial z}\right) = \frac{1}{h_{\text{sc}}}\left(\varepsilon^2\nabla_{\boldsymbol{\xi}}, \frac{\partial}{\partial z}\right) \tag{31}
$$

in terms of the dimensionless coordinates.

Based on these scalings we assess the asymptotics of the DSI_{PE}. To this end we first identify, for each of the contributing fields Θ, B, and Π their leading z-dependencies and the perturbations with full variations. This yields

$$
\begin{aligned}
\Theta &= \Theta_0 + \varepsilon\Theta_1 + \varepsilon^2\Theta^{(2)} + \mathscr{O}\left(\varepsilon^2\right) \\
\Pi &= \varepsilon^2\Pi_2 + \varepsilon^3\Pi^{(3)} + \mathscr{O}\left(\varepsilon^3\right) \\
B &= \frac{\kappa}{\kappa-1}T_0 + z + \varepsilon\frac{\kappa}{\kappa-1}T_1 + \varepsilon^2\frac{\kappa}{\kappa-1}T^{(2)} + \mathscr{O}\left(\varepsilon^2\right)
\end{aligned}
\tag{32}
$$

where the temperature functions $T_i, T^{(i)}$ result from the expansion of the identity $T = \Theta\pi$. The leading two contributions to Ertel's potential vorticity (PV) are

$$
\begin{aligned}
\Pi_2 &= \frac{f_0\Theta_1'}{\rho_0} \\
\Pi^{(3)} &= \frac{f_0\Theta_1'}{\rho_0}\left(\frac{\Theta_z^{(2)}}{\Theta_1'} - \frac{\rho_1}{\rho_0} + \frac{\zeta^{(0)} + \beta\xi_2}{f_0}\right)
\end{aligned}
\tag{33}
$$

where $\Theta_1' \equiv d\Theta_1/dz$, $\xi_2 = \varepsilon^2 y$, and where

$$
\zeta^{(0)} = \boldsymbol{k}\cdot\left(\nabla_{\boldsymbol{\xi}} \times \boldsymbol{u}^{(0)}\right)
\tag{34}
$$

is the leading order vertical vorticity. Note that $\Pi^{(3)} \neq \Pi_{\mathrm{QG}}$ is *not* the potential vorticity known from classical QG theory. The difference will become transparent shortly. For further information see the appendix, where we rederive the QG-PV transport equation straight from Ertel's PV conservation law for the full compressible Euler equations in the QG scaling regime.

Based on the representations in (31), (32), the gradients of Θ, Π, B, decomposed into their leading vertical and horizontal components, read

$$
\begin{aligned}
\nabla\Theta &= \boldsymbol{k}\sum_{j=1}^{4}\varepsilon^j\Theta_z^{(j)} + \varepsilon^4\nabla_{\boldsymbol{\xi}}\Theta^{(2)} + \mathscr{O}\left(\varepsilon^4\right) \\
\nabla\Pi &= \boldsymbol{k}\sum_{j=2}^{5}\varepsilon^j\Pi_z^{(j)} + \varepsilon^5\nabla_{\boldsymbol{\xi}}\Pi^{(3)} + \mathscr{O}\left(\varepsilon^5\right) \\
\nabla B &= \boldsymbol{k}\sum_{j=1}^{4}\varepsilon^j B_z^{(j)} + \varepsilon^4\kappa\nabla_{\boldsymbol{\xi}}T^{(2)} + \mathscr{O}\left(\varepsilon^4\right)
\end{aligned}
\tag{35}
$$

where we have momentarily dropped the lower index notation for purely z-dependent functions for convenience of notation. Note the leading contribution to the Bernoulli function, $B_0 = \frac{\kappa}{\kappa-1}T_0 + z \equiv$

$\Theta_0 = \text{const.}$, such that the expansion of ∇B starts at order $\mathscr{O}(\varepsilon)$ just as that of $\nabla\Theta$. Note also that $\nabla\Pi = \mathscr{O}\left(\varepsilon^2\right)$ instead.

We insert the expressions from (35) in the definition of the $\mathrm{DSI}_{\mathrm{PE}}$, observe that any expression $\boldsymbol{a}\cdot(\boldsymbol{b}\times\boldsymbol{c})$ in which two of the three vectors are collinear vanishes, and then find

$$\mathrm{DSI}_{\mathrm{PE}} = \varepsilon^{10}\mathrm{DSI}^{(10)} + \mathscr{O}\left(\varepsilon^{10}\right), \tag{36}$$

where

$$\mathrm{DSI}^{(10)} = \frac{\boldsymbol{k}}{\rho_0}\cdot\left(\nabla_\xi\Pi^{(3)}\times\left[\kappa T_1'\nabla_\xi\Theta^{(2)} - \Theta_1'\nabla_\xi\kappa T^{(2)}\right] - \left[\nabla_\xi\kappa T^{(2)}\times\nabla_\xi\Theta^{(2)}\right]\frac{d\Pi_2}{dz}\right). \tag{37}$$

Using $T^{(2)} = \pi_0\Theta^{(2)} + \pi^{(2)}\Theta_0 + \pi_1\Theta_1$, the expression in (37) can be simplified further to yield the leading term of the DSI in the classical QG limit. We recall (37) and collect

$$\begin{aligned} T_1' &= \pi_0'\Theta_1 + \pi_0\Theta_1' + \pi_1'\Theta_0 = -\frac{\Theta_1}{\kappa\Theta_0} + \pi_0\Theta_1' + \frac{\Theta_1\Theta_0}{\kappa\Theta_0^2} = \pi_0\Theta_1' \\ T^{(2)} &= (\Theta\pi)^{(2)} = \pi_0\Theta^{(2)} + \pi^{(2)}\Theta_0 + \pi_1\Theta_1\,. \end{aligned} \tag{38}$$

This yields

$$T_1'\nabla_\xi\Theta^{(2)} - \Theta_1'\nabla_\xi T^{(2)} = -\Theta_0\Theta_1'\nabla_\xi\pi^{(2)}\,. \tag{39}$$

From (38) we find for the second square bracket of (37)

$$\nabla_\xi\Theta^{(2)}\times\nabla_\xi T^{(2)} = \nabla_\xi\Theta^{(2)}\times\Theta_0\nabla_\xi\pi^{(2)}\,. \tag{40}$$

Finally from (37)

$$\mathrm{DSI}^{(10)} = \frac{\kappa}{\kappa-1}\frac{\Theta_1'^2}{\rho_0^2}\,\boldsymbol{k}\cdot\left(\Theta_0\nabla_\xi\pi^{(2)}\times\nabla_\xi\Pi_{\mathrm{QG}}\right) + \mathscr{O}(1)\,, \tag{41}$$

where

$$\Pi_{\mathrm{QG}} = \frac{\rho_0}{\Theta_1'}\left(\Pi^{(3)} - \frac{\Theta^{(2)}}{\Theta_1'}\frac{d\Pi_2}{dz}\right) = \zeta^{(0)} + \beta\xi_2 + \frac{f_0}{\rho_0}\left(\frac{\rho_0\Theta^{(2)}}{\Theta_1'}\right)_z \tag{42}$$

is the classical potential vorticity variable from QG theory, *i.e.*, the dimensionless version of (16). See the appendix for a detailed derivation. Thus, the asymptotic scale analysis results in a dimensionless representation of the $\mathrm{DSI}_{\mathrm{PE}}$ in the quasi-geostrophic regime. We formulate (41) in terms of the Jacobi-determinant, recalling that Θ_0 is a constant and that, by hydrostatic balance,

$$\phi^{(2)} = \frac{\kappa}{\kappa - 1} \Theta_0 \pi^{(2)} \tag{43}$$

relates the perturbations of the geopotential height and the Exner pressure. Then

$$\mathrm{DSI}^{(10)} = \frac{{\Theta_1'}^2}{\rho_0^2} \frac{\partial(\phi^{(2)}, \Pi_{\mathrm{QG}})}{\partial(\xi_1, \xi_2)} + \mathscr{O}(1) \, . \tag{44}$$

This is to be compared with the representation of $\mathrm{DSI}_{\mathrm{QG}}$ in (24) as derived by the energy-vorticity concept. To do so, we re-dimensionalize (44) by multiplication with $\varepsilon^{10}\, \mathrm{DSI}_{\mathrm{ref}}$, where

$$\mathrm{DSI}_{\mathrm{ref}} = \frac{(T_{\mathrm{ref}}/h_{\mathrm{sc}})^2}{\rho_{\mathrm{ref}}^2} \frac{(g h_{\mathrm{sc}})(u_{\mathrm{ref}}/h_{\mathrm{sc}})}{h_{\mathrm{sc}}^2} = \frac{T_{\mathrm{ref}}^2}{\rho_{\mathrm{ref}}^2} \frac{g u_{\mathrm{ref}}}{h_{\mathrm{sc}}^4} \tag{45}$$

is the unit of measure for the DSI that results from the present nondimensionalization, to obtain, dropping the superscripts for convenience of notation,

$$\varepsilon^{10} \mathrm{DSI}_{\mathrm{ref}} \mathrm{DSI}^{(10)} = \mathrm{DSI}_{\mathrm{QG}} = \frac{\overline{\Theta}'^2}{\rho_0{}^2} \frac{\partial(\phi, \Pi_{\mathrm{QG}})}{\partial(x, y)} \, . \tag{46}$$

The term on the right hand side of the last equation is the final dimensional representation of the DSI for the quasi-geostrophic model and the term on the left hand side includes the scaling aspect with respect to the meso-gamma scale of $\sim 10\,\mathrm{km}$. Furthermore, the multi-scale asymptotic-approach determines the factor μ in the representation of the Dynamic State Index $\mathrm{DSI}_{\mathrm{QG},\mu}$ from (24), derived via energy-vorticity-theory in section 3:

$$\mu = -\frac{\overline{\Theta}'^2 f_0}{\rho_0} \tag{47}$$

Thus, $\mathrm{DSI}_{\mathrm{QG},\mu}$ represents precisely the leading-order term in an asymptotic expansion of the $\mathrm{DSI}_{\mathrm{PE}}$ as derived originally from the full compressible flow equations. It seems reassuring that the DSI-theory is asymptotically self-consistent in this way.

A remark is in order as regards the factor of ε^{10} appearing in (36). According to (41), the dominant contributions to the DSI in the QG-regime result from the cross product of the horizontal gradients of the Exner pressure and Ertel's potential vorticity and from the vertical derivative of the potential temperature. According to the asymptotic expansions in (35), these terms are of orders $\varepsilon^4, \varepsilon^5$, and ε, respectively, and this explains the very high total power of ε appearing in (36).

Note also that in SI units, $[\mathrm{DSI}_{\mathrm{ref}}] \sim K^2 m^4/kg^2 s^3 = 10^{12} (PVU)^2 s^{-1}$, the latter being a natural unit for the DSI based on the primitive equations and established scalings for the potential vorticity.

c. Interpretation of $\mathrm{DSI}_{\mathrm{QG}}$

The DSI is meant to quantify imbalances in a flow field. To interpret the index in the quasi-geostrophic limit, we recall that the leading-order QG flow velocity $\boldsymbol{u}^{(0)}$ satisfies geostrophic balance, *i.e.*, $f_0 \boldsymbol{k} \times \boldsymbol{u}^{(0)} + \kappa \Theta_0 \nabla_{\xi} \pi^{(2)} = 0$, and that the QG potential vorticity is a conserved scalar, such that

$$\frac{\partial \Pi_{\mathrm{QG}}}{\partial \tau} + \boldsymbol{u}^{(0)} \cdot \nabla_{\xi} \Pi_{\mathrm{QG}} = 0\,. \tag{48}$$

With this information we can replace

$$\mathrm{DSI}^{(10)} = -\frac{\Theta_1'^{\,2}}{f_0 \rho_0^2} \frac{\partial \Pi_{\mathrm{QG}}}{\partial \tau}\,, \tag{49}$$

and find that, indeed, the DSI naturally captures the advection-induced nonstationarity encoded in the QG-dynamics.

d. The $\mathrm{DSI}_{\mathrm{QG}}$ *derived from zero steady wind mass flux divergence*

Going back to section 2b, we consider here the leading-order asymptotics of the steady wind field (7) in the QG-regime. Recalling (32), (33), (35) and (39), keeping only those terms that ultimately count for the leading-order contributions to the $\mathrm{DSI}_{\mathrm{QG}}$, and using the present dimensionless representation we find

$$\begin{aligned}\rho \mathbf{v}_{st}^{\mathrm{QG}} = &\ \frac{\varepsilon^{-3}}{\varepsilon^2\Pi_2+\varepsilon^3\Pi^{(3)}}\left(\left(\varepsilon\Theta_1'\boldsymbol{k}+\varepsilon^4\nabla_\xi\Theta^{(2)}\right)\times\left(\frac{\kappa}{\kappa-1}\left[\varepsilon T_1'\boldsymbol{k}+\varepsilon^4\nabla_\xi T^{(2)}\right]\right)\right)+\text{h.o.t.}\\ = &\ \frac{\Theta_1'}{\Pi_2}\boldsymbol{k}\times\frac{\kappa\Theta_0}{\kappa-1}\nabla_\xi\pi^{(2)}+\text{h.o.t.}=\rho_0\boldsymbol{u}^{(0)}+\text{h.o.t.}\end{aligned} \tag{50}$$

Thus, at *leading order* the stationary wind matches the geostrophic wind. Note that the scaling factor of ε^{-3} in the first line of (50) results from the product of the units of measure that define the stationary wind. Denoting dimensional variables by an asterisk again, we have

$$\nabla^*\Theta^* = \frac{T_{\mathrm{ref}}}{h_{\mathrm{sc}}}\nabla\Theta\,,\quad \nabla^*B^* = \frac{RT_{\mathrm{ref}}}{h_{\mathrm{sc}}}\nabla B\,,\quad \Pi^* = \frac{\nabla^*\Theta^*\cdot(\nabla^*\times\boldsymbol{v}^*)}{\rho^*} = \frac{T_{\mathrm{ref}}u_{\mathrm{ref}}}{\rho_{\mathrm{ref}}h_{\mathrm{sc}}^2}\frac{\nabla\Theta\cdot(\nabla\times\boldsymbol{v})}{\rho} \tag{51}$$

and, collecting all terms from the definition of the stationary wind,

$$(\rho\mathbf{v}_{st})^* = \frac{RT_{\mathrm{ref}}}{u_{\mathrm{ref}}^2}\rho_{\mathrm{ref}}u_{\mathrm{ref}}\frac{1}{\Pi}\nabla\Theta\times\nabla B = \frac{1}{\varepsilon^3}\rho_{\mathrm{ref}}u_{\mathrm{ref}}\frac{1}{\Pi}\nabla\Theta\times\nabla B\,. \tag{52}$$

With (33) and (43), i.e. $\Pi_2 = \frac{f_0\Theta_1'}{\rho_0}$ and $\phi^{(2)} = \frac{\kappa\Theta_0}{\kappa-1}\pi^{(2)}$, last equation results in

$$\left(\rho\mathbf{v}_{st}^{\mathrm{QG}}\right)^{(0)} = \rho_0\frac{1}{f_0}\boldsymbol{k}\times\nabla\phi\,. \tag{53}$$

This may seem puzzling at first, because clearly $\nabla\cdot\left(\rho_0\mathbf{v}_{st}^{\mathrm{qg}}\right)^{(0)}\equiv 0$ by construction, and thus the corresponding "leading order DSI" would vanish identically. The resolution of the puzzle lies in the fact that the two calculational steps involved do not commute. The divergence of the leading order field does generally not equal the leading order divergence of the full field. To arrive at the $\mathrm{DSI}_{\mathrm{QG}}$ as derived in (44) along a different path before, we carefully expand the divergence of the expression in the first line of (50). This yields

$$\begin{aligned}-\nabla\cdot(\rho\mathbf{v}_{st}) = \frac{\boldsymbol{k}}{\kappa-1}\left[\nabla_\xi\Pi^{(3)}\times\left(\kappa T_1'\nabla_\xi\Theta^{(2)}-\Theta_1'\nabla_\xi\kappa T^{(2)}\right)-\frac{d\Pi_2}{dz}\left(\nabla_\xi\kappa T^{(2)}\times\nabla_\xi\Theta^{(2)}\right)\right]\\ +\ \text{h.o.t.}\end{aligned} \tag{54}$$

after some straightforward manipulations. As expected, this is the same expression we obtained for $\mathrm{DSI}^{(10)}$ in (37) above, up to the scalar prefactor $(\kappa-1)\rho_0^{-1}$.

5. Scale dependent analysis of precipitation in terms of the two DSI parameters

The DSI for the primitive equations as well as the DSI for the quasi-geostrophic model describe deviations from a steady, adiabatic and inviscid basic state. However, the basic states are given by different steady wind solutions depending on the model approximation of the atmospheric flow field. Especially the strength and spatial structure of diabatic processes related to precipitation processes can be compared by the two Dynamic State Indices. Therefore, we will analyze the two indices $|\mathrm{DSI}_{\mathrm{PE}}|$ and $|\mathrm{DSI}_{\mathrm{QG}}|$ with the focus to evaluate the skill to diagnose precipitation processes. For the calculation of the different DSI's as well as for the precipitation fields hourly COMSO-DE data of the German Weather Service in June, July and August 2007 with a horizontal resolution of 2.8 km id used (Schättler et al. 2008). Applying central differences, the Dynamic State Indices are determined on 11 pressure surfaces (200, 250, 300, 400, 500, 600, 700, 850, 950, 975 and 1000 hPa) for each grid box.

a. Comparing the horizontal structures of $\mathrm{DSI}_{\mathrm{PE}}$ *and* $\mathrm{DSI}_{\mathrm{QG}}$

In the following we will examine the two parameters $|\mathrm{DSI}_{\mathrm{PE}}|$ and $|\mathrm{DSI}_{\mathrm{QG}}|$ based on the COSMO-DE data set. Previous works have shown high correlation of the $|\mathrm{DSI}_{\mathrm{PE}}|$ with precipitation (see e.g. Claussnitzer et al. (2008)). In fig. 2 the time series of $|\mathrm{DSI}_{\mathrm{PE}}|$ (red curve) and precipitation (blue curve), hourly averaged over Germany in June, July and August 2007 is illustrated. For this time period that is characterized by numerous convective precipitation events with high intensity a Spearman's rank coefficient of the DSI with precipitation of 0.82 was found. The spatial structure of both DSI parameters for July 20th 2007 and the corresponding radar image provided by the German Weather Service (DWD) is shown in fig. 3 and fig. 4. On this day, a frontal precipitation band was crossing Germany. The numerical evaluation of both DSI parameters depict the elongated structure of the front. The $\mathrm{DSI}_{\mathrm{PE}}$-field shows a connected band of smaller scale cellular structures with negative values on the front side and positive values on the back side of the front. In contrast, the structure of the $\mathrm{DSI_{QG}}$ depict more disconnected, larger areas of precipitation. $\mathrm{DSI_{QG}}$ provides deviations of the geostrophic wind only based on geopotential hight field fluctuations reflecting larger scale diabatic processes. The $\mathrm{DSI_{PE}}$ is based on the fluctuations of geopotential height field but additionally of the variables of the three wind components and the temperature field and thus it can describe the smaller scale structures characterized by higher intensity of precipitation.

A direct comparison of the DSI for the quasi-geostrophic model and the DSI for the primitive equations with respect to precipitation is illustrated in the scatter plot in fig. 5. Hereby 6 hourly COSMO-DE date for June and July 2007 was used to calculate the two DSI indices that are divided by their standard derivation to draw a better comparison. The red dots show the time steps with a precipitation threshold of 1 mm/h which is equivalent to the 88th percentile and the blue dots mark the DSI-parameters below this threshold. All values are located near the bisecting line. Small values of both DSI parameters are related to less precipitation, whereas high DSI values occur on time steps with precipitation above the precipitation threshold of 1 mm/h. For strong precipitation there are more events above the bisecting line indicating higher $\mathrm{DSI_{PE}}$-values compared to $\mathrm{DSI_{QG}}$ values. The opposite holds for events characterized by less precipitation. Thus we notice that the $\mathrm{DSI_{PE}}$ provides the possibility to capture extreme precipitation events.

b. Comparing the vertical structure of $|\mathrm{DSI_{PE}}|$ *and* $|\mathrm{DSI_{QG}}|$ *with respect to precipitation*

To evaluate the vertical structure of the Dynamic State Index with respect to precipitation, we divide the domain into regions with and without precipitation and compare the two DSI parameters for these regions. In fig. 6 the vertical profiles of the the two Dynamic State Indices are investigated for July 20th 2007 using 3-hourly COSMO-DE data set. On this day a cold front of the low pressure system Dietmar II passed Germany which lead to high precipitation. The radar image and the horizontal structure of the DSI are shown in fig. 3 and fig. 4. This case has also been analyzed during the intensive observation period (IOP-9c) of the convective and orographically-induced precipitation study (COPS), see Schwitalla et al. (2011). For every time step and every pressure level we divide the DSI-values into two classes; one class for absolute DSI values in grid boxes with precipitation and the other class contains all absolute DSI values without precipitation. Then, we calculate the arithmetic mean on each pressure level for each class. We norm the indices by dividing all values in a particular class by the mean of this class. The result is shown in fig. 6. The solid lines show the vertical DSI profile for the different models on grid boxes with precipitation and the dashed lines show the DSI values for grid boxes without precipitation. First, we compare the vertical profile of the indices $|\mathrm{DSI}_{\mathrm{PE}}|$ and $|\mathrm{DSI}_{\mathrm{QG}}|$. The DSI based on the primitive equations has larger values compared to $\mathrm{DSI}_{\mathrm{QG}}$ which is accordance with the result of the multi-scale asymptotic (44). These different order of magnitudes can be explained by the different sensibilities of the models: The $\mathrm{DSI}_{\mathrm{PE}}$ based on the primitive equation involves five variables, the three dimensional wind, the potential temperature and the geopotential field. Therefore, already small changes of one of the variables affect the DSI leading to large variations of $\mathrm{DSI}_{\mathrm{PE}}$ in the vertical profile. On the other hand, $\mathrm{DSI}_{\mathrm{QG}}$ only involves the geopotential field and the stratification leading to small variations. The sensibilities are due to the deviations of two different basic state solutions, where the larger fluctuations around the steady wind solution of the primitive equations can reflect stronger turbulent processes.

The DSI values of both indices with precipitation (solid lines) are higher than the DSI values without precipitation (dashed lines), where the enclosed area between the curves with and without precipitation decreases for the QG-model. Enclosing the largest area between 600 hPa and 400 hPa the $\mathrm{DSI}_{\mathrm{PE}}$ has the best skill to diagnose precipitation processes. It has to be noted that we calculated the two DSI parameters with the data set of the COSMO-DE model which is based on the primitive equations and explicitly resolves deep convection. Even though the order of magnitude of $\mathrm{DSI}_{\mathrm{QG}}$ is small and might be numerical subtle, we obtain a Spearman rank correlation of 0.76 with precipitation. Thus, the analysis of the vertical structure of the two Dynamic State Indices shows the height where the generation of precipitation is predominant.

6. Conclusions

In this paper, we have shown that the concept of the Dynamic State Index (DSI) can be transferred to different fluid mechanical models starting with the original primitive equations through two complementary approaches. For all scales, the DSI describes non-stationary, diabatic, and dissipative processes by capturing local deviations from a steady and adiabatic wind solution. However, which field is to be considered as a steady adiabatic wind depends on the considered flow model. Using two different theoretical approaches we have derived the $\mathrm{DSI}_{\mathrm{QG}}$ for the quasi-geostrophic model which is a benchmark model for the understanding of large scale atmospheric dynamics. One derivation is based on ideas provided by the Energy-Vorticity-Theory for ideal fluid mechanics, in the second we have analyzed the structure of the original $\mathrm{DSI}_{\mathrm{PE}}$ based on the primitive equations in the quasi-geostrophic limit by asymptotic techniques. While the derivation of the $\mathrm{DSI}_{\mathrm{QG}}$ by the Energy-Vorticity Theory provides the general physical representation of the $\mathrm{DSI}_{\mathrm{QG}}$, using asymptotic scale analysis corroborates the result and even determines a scalar factor providing the same dimension as the $\mathrm{DSI}_{\mathrm{PE}}$. Starting with the $\mathrm{DSI}_{\mathrm{PE}}$ on the meso-gamma scale of $\sim 10\,\mathrm{km}$ as a reference and using the synoptic flow Rossby number $\mathrm{Ro} = \varepsilon \ll 1$, the $\mathrm{DSI}_{\mathrm{PE}}$ evaluated on synoptic-scale geostrophically balanced data scales as ε^{10}. Thus, through two conceptually independent procedures, we have established the DSI index for QG-flows that is both the asymptotic leading order approximation to the $\mathrm{DSI}_{\mathrm{PE}}$ and a proper Dynamic State Index in the sense of the Energy-Vorticity-Theory.

Comparing $\mathrm{DSI}_{\mathrm{PE}}$ and $\mathrm{DSI}_{\mathrm{QG}}$ with respect to precipitation, the $\mathrm{DSI}_{\mathrm{PE}}$ signal reflects small scale cellular structures characterized by higher intensity of precipitation on the convective scales. The $\mathrm{DSI}_{\mathrm{QG}}$ shows meso-scale clusters related to extended precipitation structures. With respect to future work, we note that the unit measure for the DSI which results from nondimensionalization implies a novel, non-equilibrium time scale combining the potential vorticity, PV, and the DSI. The statistics of this implied time scale across the spacial scales of the atmosphere may provide interesting new guidelines for the interpretation of observational data.

To summarize, the DSI parameter reflects model dependent deviations of the non-linear solution of atmospheric equations. Therefore, the DSI is a skillful dynamical concept that provides a scale-dependent diagnosis of irreversible processes and helps for a better understanding of diabatic atmospheric phenomena which dominate the non-resolved scales.

Acknowledgments. A. MÜLLER, P. NÉVIR, and R. KLEIN thank Deutsche Forschungsgemeinschaft for their support within the framework of CRC 1114 "Scaling Cascades in Complex Systems", projects A01, A02 and C06. The authors also thank Henning Rust, Christoph Ritschel for helpful discussions and Alexander Pasternack for providing fig. 1.

APPENDIX

A1. Derivation of the DSI-QG by the Energy-Vorticity Theory

To determine the functional derivative of the total energy $\mathscr{H}_{QG}$ of the QG-model, first we calculate its variation:

$$\begin{aligned}\delta\mathscr{H}_{QG} &= \frac{1}{f_0^2}\int_m \left(\tilde{\boldsymbol{\nabla}}\phi\cdot\delta\tilde{\boldsymbol{\nabla}}\phi\right)\, dm \\ &= \frac{1}{f_0^2}\int_m \left(-\phi\delta\tilde{\boldsymbol{\nabla}}\cdot\tilde{\boldsymbol{\nabla}}\phi\right) + \frac{1}{f_0^2}\int_m \tilde{\boldsymbol{\nabla}}\cdot\left(\phi\delta\tilde{\boldsymbol{\nabla}}\phi\right)\, dm \\ &= -\frac{1}{f_0}\int_m \left(\phi\delta\Pi_{\mathrm{QG}}\right)\, dm\end{aligned} \tag{A1}$$

where we assume suitable boundary conditions and apply Gauss' divergence theorem such that in the second line the second summand vanishes. Then, the functional derivative of the energy reads as:

$$\frac{\delta\mathscr{H}_{QG}}{\delta\Pi_{\mathrm{QG}}} = -\frac{\phi}{f0} \tag{A2}$$

We note that the definitions of the scalar product and gradient given in (18) and (19) were used.

A2. The QG regime

a. QG scalings for Ertel's potential vorticity

According to (32) the dimensionless Bernoulli function is dominated in the QG regime up to and including second order by the thermodynamic enthalpy $e + p/\rho = \kappa T$ and the geopotential z. This justifies the representation of the leading order dependencies for ∇B in (35), since

$$T = T_0(z) + \varepsilon T_1(z) + \varepsilon^2 T^{(2)}(\tau,\boldsymbol{\xi},z) + \mathscr{O}\left(\varepsilon^2\right)\,, \tag{A3}$$

so that the leading horizontal gradient term is $\varepsilon^4\nabla_{\boldsymbol{\xi}}T^{(2)}$, while all other gradient contributions up to and including order ε^4 are vertically oriented, *i.e.*, they are proportional to $\boldsymbol{k}$.

To corroborate the expression for $\Pi^{(3)}$ in (33) we observe that

$$
\begin{aligned}
\nabla\times\boldsymbol{v} &= (\varepsilon^2\nabla_{\boldsymbol{\xi}}+\boldsymbol{k}\partial_z)\times\sum_{i=0}^{2}\varepsilon^i\boldsymbol{u}^{(i)}+\mathscr{O}\left(\varepsilon^2\right)\\
&= \sum_{i=0}^{2}\varepsilon^i\boldsymbol{k}\times\boldsymbol{u}_z^{(i)}+\varepsilon^2\nabla_{\boldsymbol{\xi}}\times u^{(0)}+\mathscr{O}\left(\varepsilon^2\right)
\end{aligned}
\tag{A4}
$$

and that the first term on the right is horizontal while the second points in the vertical direction. Using the decomposition of $\nabla\Theta$ from (35) we readily verify (33). Consider now the Ertel's potential vorticity,

$$
\Pi=\frac{1}{\rho}(\nabla\times\boldsymbol{v}+2\boldsymbol{\Omega})\cdot\nabla\Theta
\tag{A5}
$$

Asymptotic expansion of this expression yields, neglecting higher order terms,

$$
\begin{aligned}
\frac{1}{\rho} &= \frac{1}{\rho_0}-\varepsilon\frac{\rho_1}{\rho_0^2}+\varepsilon^2\left[\frac{1}{2}\frac{\rho_1^2}{\rho_0^3}-\frac{\rho^{(2)}}{\rho_0^2}\right]\\
\nabla\times\boldsymbol{v} &= \sum_{i=0}^{2}\varepsilon^i\boldsymbol{k}\times\boldsymbol{u}_z^{(i)}+\varepsilon^2\nabla_{\boldsymbol{\xi}}\times\boldsymbol{u}^{(0)}\\
2\boldsymbol{\Omega} &= \boldsymbol{k}\left(\varepsilon f_0+\varepsilon^2\beta\xi_2\right)\\
\nabla\Theta &= \sum_{i=1}^{4}\varepsilon^i\boldsymbol{k}\Theta_z^{(i)}+\varepsilon^4\nabla_{\boldsymbol{\xi}}\Theta^{(2)}
\end{aligned}
\tag{A6}
$$

Upon insertion into (A5),

$$
\begin{aligned}
\Pi =&\frac{\varepsilon}{\rho_0}\,\boldsymbol{u}_z^{(0)}\cdot\boldsymbol{k}\;\Theta_1'+\frac{\varepsilon^2}{\rho_0}\Big(f_0\Theta_1'+\boldsymbol{u}_z^{(1)}\cdot\boldsymbol{k}\;\Theta_1'+\boldsymbol{u}_z^{(0)}\cdot\boldsymbol{k}\;\left(\Theta_z^{(2)}-\frac{\rho_1}{\rho_0}\Theta_1'\right)\Big)\\
&+\frac{\varepsilon^3}{\rho_0}\Big\{f_0\left[\Theta_z^{(2)}-\frac{\rho_1}{\rho_0}\Theta_1'\right]+\left(\nabla_{\boldsymbol{\xi}}\times\boldsymbol{u}^{(0)}+\beta\xi_2\right)\Theta_1'\quad+\boldsymbol{u}_z^{(2)}\cdot\boldsymbol{k}\;\Theta_1'\\
&+\boldsymbol{u}_z^{(1)}\cdot\boldsymbol{k}\;\left(\Theta_z^{(2)}-\frac{\rho_1}{\rho_0}\Theta_1'\right)+\boldsymbol{u}_z^{(0)}\cdot\boldsymbol{k}\;\left(\Theta_z^{(3)}-\frac{\rho_1}{\rho_0}\Theta_z^{(2)}+\left[\frac{{\rho^{(1)}}^2}{2\rho_0^2}-\frac{\rho^{(2)}}{\rho_0}\right]\Theta_1'\right)\Big\}\\
&+\mathscr{O}\left(\varepsilon^3\right)
\end{aligned}
\tag{A7}
$$

Noting that $\boldsymbol{u}_z^{(i)}\cdot\boldsymbol{k}\equiv 0$, this expansion reduces to

$$
\begin{aligned}
\Pi &= \varepsilon^2\Pi_2+\varepsilon^3\Pi^{(3)}+\mathscr{O}\left(\varepsilon^3\right)\\
\Pi_2 &= \frac{f_0\Theta_1'}{\rho_0}\\
\Pi^{(3)} &= \frac{f_0\Theta_1'}{\rho_0}\left(\frac{\Theta_z^{(2)}}{\Theta_1'}-\frac{\rho_1}{\rho_0}+\frac{\zeta^{(0)}+\beta\xi_2}{f_0}\right)
\end{aligned}
\tag{A8}
$$

where

$$\zeta^{(0)} = \boldsymbol{k} \cdot \left(\nabla_{\boldsymbol{\xi}} \times \boldsymbol{u}^{(0)} \right) \tag{A9}$$

b. The QG PV transport equation

With the basic scalings in (28) and this expansion for PV, the leading-order expression for Ertel's PV conservation law yields at order ε^5

$$\left(\partial_\tau + \boldsymbol{u}^{(0)} \cdot \nabla_{\boldsymbol{\xi}} \right) \Pi^{(3)} + w^{(3)} \frac{d\Pi_2}{dz} = 0 \tag{A10}$$

from which we need to eliminate the vertical advection term for Π_2 to arrive at a single scalar transport equation for some PV variable. To this end we recall from the original QG derivations the perturbation potential temperature equation

$$\left(\partial_\tau + \boldsymbol{u}^{(0)} \cdot \nabla_{\boldsymbol{\xi}} \right) \Theta^{(2)} + w^{(3)} \Theta_1' = 0 \tag{A11}$$

which yields

$$w^{(3)} = -\frac{1}{\Theta_1'} \left(\partial_\tau + \boldsymbol{u}^{(0)} \cdot \nabla_{\boldsymbol{\xi}} \right) \Theta^{(2)} . \tag{A12}$$

Going back to (A10) and observing that Π_2 depends neither on τ nor on $\boldsymbol{\xi}$ we obtain

$$\left(\partial_\tau + \boldsymbol{u}^{(0)} \cdot \nabla_{\boldsymbol{\xi}} \right) \left(\Pi^{(3)} - \frac{\Theta^{(2)}}{\Theta_1'} \frac{d\Pi_2}{dz} \right) = 0 . \tag{A13}$$

We wish to further analyze the advected quantity in this equation. Going back to the definitions of Π_2 and $\Pi^{(3)}$ in (A8) and collecting only term involving $\Theta^{(2)}$, we combine it with the last term in (A13) to obtain

$$\frac{f_0 \Theta_z^{(2)}}{\rho_0} - \frac{\Theta^{(2)}}{\Theta_1'} \frac{d\Pi_2}{dz} = \frac{f_0 \Theta_z^{(2)}}{\rho_0} - \frac{f_0 \Theta^{(2)}}{\Theta_1'} \frac{d}{dz} \frac{\Theta_1'}{\rho_0} = \frac{f_0 \Theta_1'}{\rho_0} \frac{1}{\rho_0} \left(\frac{\rho_0 \Theta^{(2)}}{\Theta_1'} \right)_z \tag{A14}$$

Collecting these results and eliminating the time and horizontal derivatives of the purely z-dependent functions Θ_1'/ρ_0 and ρ_1/ρ_0, we may rewrite (A13) as

$$\left(\partial_\tau + \boldsymbol{u}^{(0)} \cdot \nabla_{\boldsymbol{\xi}} \right) \Pi_{\mathrm{QG}} = 0 \tag{A15}$$

where

$$\Pi_{\mathrm{QG}} = \zeta^{(0)} + \beta \xi_2 + \frac{f_0}{\rho_0} \left(\frac{\rho_0 \Theta^{(2)}}{\Theta_1'} \right)_z , \tag{A16}$$

and this is the quasi-geostrophic potential vorticity as obtained in classical derivations (Pedlosky 1992; Klein et al. 2011).

References

Allan, R. P., and B. J. Soden, 2008: Atmospheric warming and the amplification of precipitation extremes. *Science*, **321 (5895)**, 1481–1484, doi:10.1126/science.1160787.

Blender, R., 2005: Eulerian velocity reconstruction in ideal atmospheric dynamics using potential vorticity and potential temperature. *J. Phys.A: Math. Gen.*, **38 (28)**, 6419, doi:10.1088/0305-4470/38/28/014.

Butchart, N., K. Haines, and J. Marshall, 1989: A theoretical and diagnostic study of solitary waves and atmospheric blocking. *J. Atmos. Sci.*, **46 (13)**, 2063–2078.

Claussnitzer, A., 2010: Statistisch-dynamische Analyse skalenabhängiger Niederschlagsprozesse: Vergleich zwischen Beobachtungen und Modell. Ph.D. thesis, Freie Universität Berlin.

Claussnitzer, A., and P. Névir, 2009: Analysis of quantitative precipitation forecasts using the dynamic state index. *Atmos. Res.*, **94 (4)**, 694–703, doi:10.1016/j.atmosres.2009.08.013.

Claussnitzer, A., P. Névir, I. Langer, E. Reimer, and U. Cubasch, 2008: Scale-dependent analyses of precipitation forecasts and cloud properties using the dynamic state index. *Meteorol. Z.*, **17 (6)**, 813–825, doi:10.1127/0941-2948/2008/0346.

Claussnitzer, A., T. Schartner, P. Névir, K. Stephan, and U. Cubasch, 2011: The data assimilation method "latent heat nudging" assessed with the dynamic state index. *Meteorol. Z.*, **20 (2)**, 165–172, doi:10.1127/0941-2948/2011/0220.

Gaßmann, A., 2014: Deviations from a general nonlinear wind balance: Local and zonal-mean perspectives. *Meteorol. Z.*, 467–481, doi:10.1127/metz/2014/0568.

Klein, R., 2010: Scale-dependent models for atmospheric flows. *Annu. Rev. Fluid Mech.*, **42**, 249–274, doi:10.1146/annurev-fluid-121108-145537.

Klein, R., S. Vater, E. Päschke, and D. Ruprecht, 2011: Multiple scales methods in meteorology. *Asymptotic Methods in Fluid Mechanics: Survey and Recent Advances*, H. Steinrück, Ed., Springer-Verlag, CISM International Centre for Mechanical Sciences, Vol. 523, 127–196.

Martius, O., S. Pfahl, and C. Chevalier, 2016: A global quantification of compound precipitation and wind extremes. *Geophys. Res. Lett.*, **43 (14)**, 7709–7717, doi:10.1002/2016GL070017.

Névir, P., 1998: *Die Nambu-Felddarstellungen der Hydro-Thermodynamik und ihre Bedeutung für die dynamische Meteorologie*. Habilitation dissertation, FU Berlin.

Névir, P., 2004: Ertel's vorticity theorems, the particle relabelling symmetry and the energy-vorticity theory of fluid mechanics. *Meteorol. Z.*, **13 (6)**, 485–498, doi:10.1127/0941-2948/2004/0013-0485.

Névir, P., and M. Sommer, 2009: Energy-vorticity theory of ideal fluid mechanics. *J. Atmos. Sci*, **66 (7)**, 2073–2084, doi:10.1175/2008JAS2897.1.

Pedlosky, J., 1992: *Geophysical Fluid Dynamics*. 2nd ed., Springer, Berlin, Heidelberg, New York, 710 pp.

Saji, N., B. Goswami, P. Vinayachandran, and T. Yamagata, 1999: A dipole mode in the tropical indian ocean. *Nature*, **401 (6751)**, 360.

Schär, C., 1993: A generalization of Bernoulli's theorem. *J. Atmos. Sci.*, **50 (10)**, 1437–1443, doi:10.1175/1520-0469(1993)050⟨1437:AGOBT⟩2.0.CO;2.

Schättler, U., G. Doms, and C. Schraff, 2008: A description of the nonhydrostatic regional cosmo-model. part vii: user's guide. *Deutscher Wetterdienst Rep. COSMO-Model*, **4**, 142.

Schwitalla, T., H.-S. Bauer, V. Wulfmeyer, and F. Aoshima, 2011: High-resolution simulation over central europe: assimilation experiments during cops iop 9c. *Q. J. R. Meteor. Soc.*, **137 (S1)**, 156–175, doi:10.1002/qj.721.

Weber, T., and P. Névir, 2008: Storm tracks and cyclone development using the theoretical concept of the dynamic state index (dsi). *Tellus A*, **60 (1)**, 1–10, doi:10.3402/tellusa.v60i1.15266.

Weijenborg, C., P. Friederichs, and A. Hense, 2015: Organisation of potential vorticity on the mesoscale during deep moist convection. *Tellus A*, **67**, doi:10.3402/tellusa.v67.25705.

LIST OF TABLES

TABLE 1. Universal characteristics of atmospheric motions.

Earth's radius	a	$=$	$6 \cdot 10^6$	m
Earth's rotation rate	Ω	$\sim$	10^{-4}	s^{-1}
Acceleration of gravity	g	$=$	9.81	ms^{-2}
Sea level pressure	p_{ref}	$=$	10^5	$\mathrm{kgm}^{-1}\mathrm{s}^{-2}$
Temperature	T_{ref}	$\sim$	273	K
Pot. temp. variation	$\Delta\Theta$	$\sim$	40	K
Dry gas constant	R	$=$	287	$\mathrm{m}^2\mathrm{s}^{-2}\mathrm{K}^{-1}$
Dry isentropic exponent	γ	$=$	1.4	

TABLE 2. Auxiliary reference quantities derived from those in table 1.

density	ρ_{ref}	$=$	$p_{\text{ref}}/(R\,T_{\text{ref}})$	$\sim$	1.25	kgm^{-3}
scale height	h_{sc}	$=$	$p_{\text{ref}}/(g\,\rho_{\text{ref}})$	$\sim$	8	km
sound speed	c_{ac}	$=$	$\sqrt{\gamma p_{\text{ref}}/\rho_{\text{ref}}}$	$\sim$	330	ms^{-1}
ext. wave speed	c_{ext}	$=$	$\sqrt{g h_{\text{sc}}}$	$\sim$	280	ms^{-1}
int. wave speed	c_{int}	$=$	$\sqrt{g h_{\text{sc}} \dfrac{\Delta\Theta}{T_{\text{ref}}}}$	$\sim$	110	ms^{-1}
thermal wind	u_{th}	$=$	$\dfrac{2}{\pi} \dfrac{g h_{\text{sc}}}{\Omega a} \dfrac{\Delta\Theta}{T_{\text{ref}}}$	$\sim$	12	ms^{-1}

LIST OF FIGURES

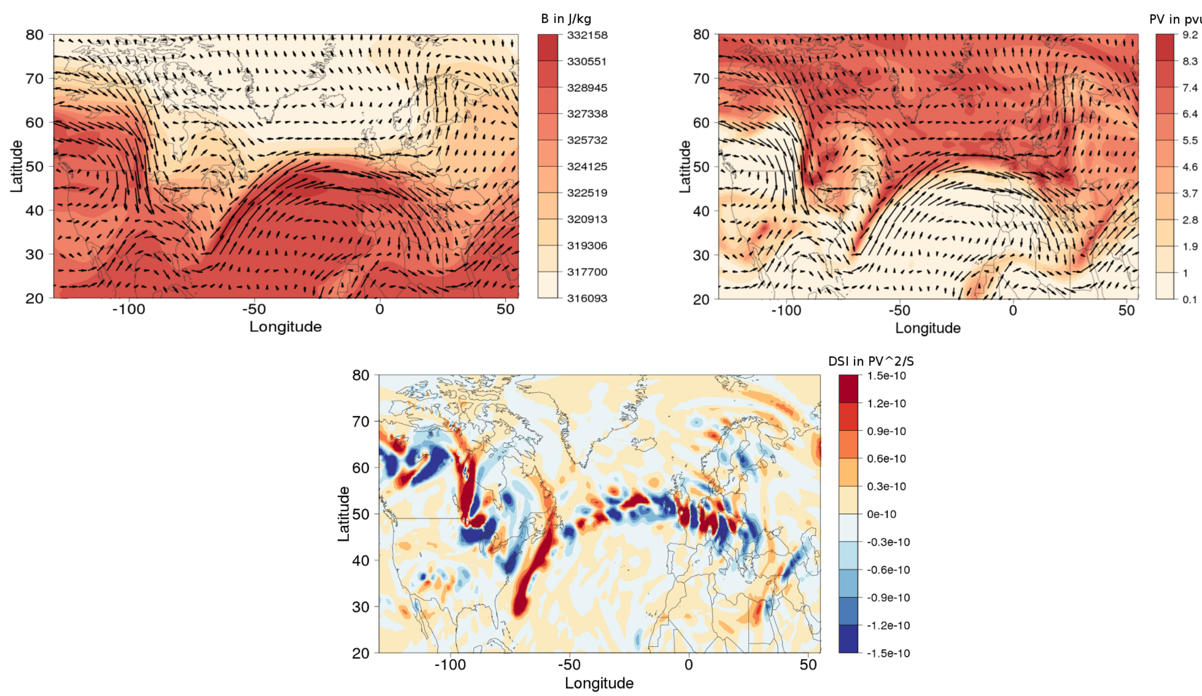

FIG. 1. The wind field and the Bernoulli function (upper left), the wind field and Ertel's PV (upper right) and the DSI-dipole structure (lower panel) are shown. In regions where the wind crosses the Bernoulli function, respectively Ertel's PV, DSI-dipole structures can be observed.

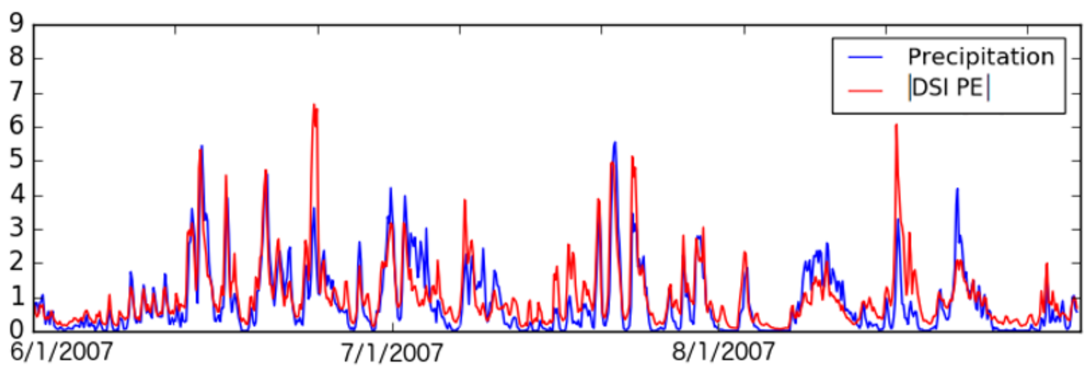

560 FIG. 2. The time series of the mean $|\mathrm{DSI}_{\mathrm{PE}}|$ in 600 hPa and mean precipitation divided by their standard

561 deviations, JJA 2007, Germany, COSMO-DE showing a high correlation.

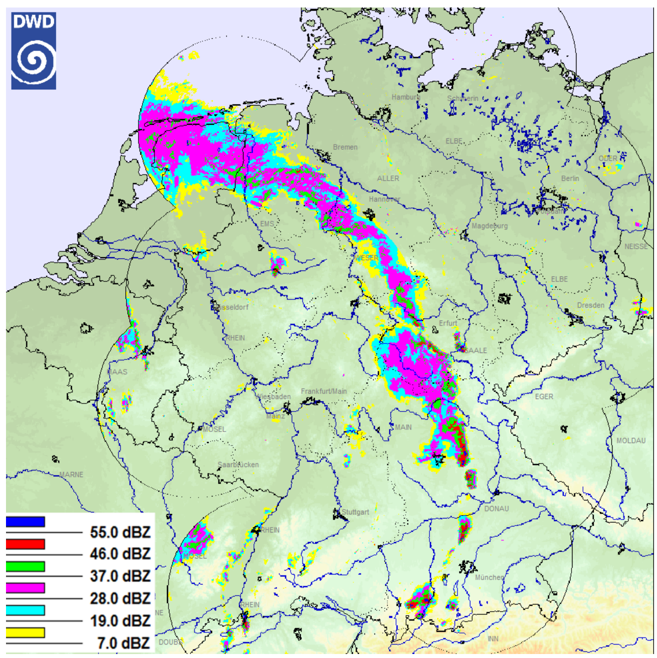

FIG. 3. Radar image for July 20th 2007, 15 UTC, Germany, adapted with courtesy of the German Weather Service (DWD)

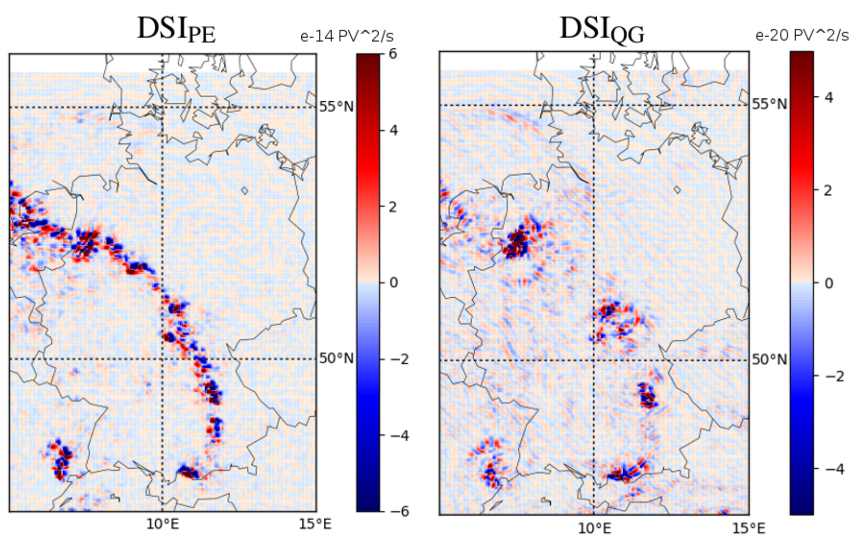

FIG. 4. The spatial horizontal structure of DSI_{PE} and $\mathrm{DSI}_{\mathrm{QG}}$ are shown for July 20th 2007, 15 UTC, 600 hPa, indicating the frontal structure shown in fig. 3.

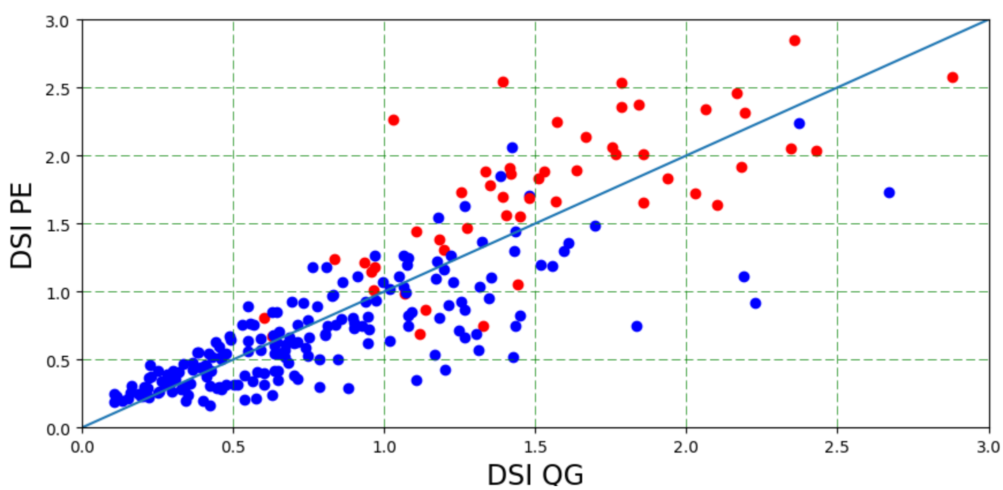

FIG. 5. The dots show the values of DSI_{QG} and DSI_{PE} for each time step calculated for the 6-hourly data set of COSMO-DE for July and August 2007. The red dots show the DSI values for high precipitation, where a threshold of the 88th percentile was taken.

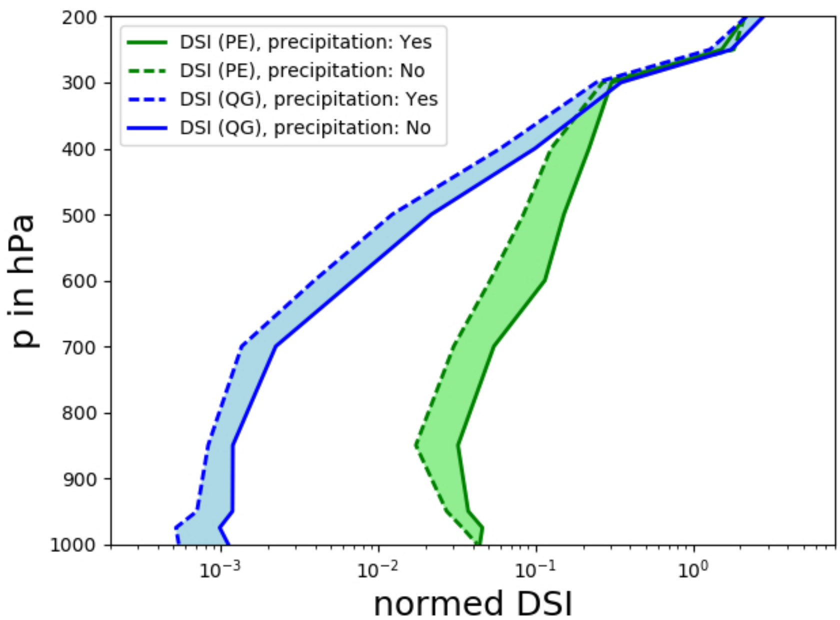

569 FIG. 6. The vertical profile of DSI_{QG} and DSI_{PE} are shown. The solid lines show the vertical DSI profiles for the different models on grid boxes with precipitation and the dashed lines show the DSI values for grid boxes without precipitation. The COSMO-DE data set for July 20th 2007, 3 hourly, was used.